Combined effects of photoaging and natural organic matter on the colloidal stability of nanoplastics in aquatic environments

Xu, Y.; Ou, Q.; Li, Xiaoming; Wang, Xintu; van der Hoek, J.P.; Liu, Gang

DOI
10.1016/j.watres.2022.119313

Publication date
2022

Document Version
Final published version

Published in
Water Research

Water Research 226 (2022) 119313

Contents lists available at ScienceDirect

Water Research

journal homepage: www.elsevier.com/locate/watres

Combined effects of photoaging and natural organic matter on the colloidal stability of nanoplastics in aquatic environments

Yanghui Xu [a,b], Qin Ou [a,b], Xiaoming Li [a,c], Xintu Wang [a,d], Jan Peter van der Hoek [b,e], Gang Liu [a,c,*]

[a] Key Laboratory of Drinking Water Science and Technology, Research Centre for Eco-Environmental Sciences, Chinese Academy of Sciences, Beijing, 100085, PR China
[b] Section of Sanitary Engineering, Department of Water Management, Faculty of Civil Engineering and Geosciences, Delft University of Technology, Stevinweg 1, 2628 CN Delft, The Netherlands
[c] University of Chinese Academy of Sciences, Beijing, China
[d] College of Environmental Science and Engineering, Guilin University of Technology, Guangxi 541004, China
[e] Waternet, Department Research & Innovation, P.O. Box 94370, 1090 GJ Amsterdam, the Netherlands

ARTICLE INFO

Keywords:
Nanoplastics
Colloidal stability
Natural organic matter
Photoaging
Steric repulsion
Photo-flocculation

ABSTRACT

The transport and fate of nanoplastics (NPs) in aquatic environments are closely associated with their colloidal stability, which is affected by aging and natural organic matter (NOM) adsorption. This study systematically investigated the combined effects of photoaging and NOM (e.g. humic acids, HA; and a model protein, bovine serum albumin, BSA) on the aggregation kinetics of NPs (polystyrene, PS) in NaCl and $CaCl_2$ solutions. Our results showed that photoaged NPs adsorbed less HA than pristine NPs due to weaker hydrophobic and π-π interactions. In return, HA showed weaker impacts on NPs' stability after photoaging. Differently, photoaged NPs absorbed more BSA than pristine NPs due to stronger hydrogen bonding and electrostatic attraction. Thus, the inhibitory effects of BSA on the aggregation kinetics of NPs were enhanced after photoaging. Regarding the effects of NOM on the aging of NPs, our results showed that HA competed with NPs for photons and underwent photo-degradation. Subsequently, the destruction/reconstruction of adsorbed HA increased (in NaCl) or decreased (in $CaCl_2$) the stability of NPs. Notably, light radiation-induced flocculation of BSA molecules, which wrapped and integrated NPs and lead to their destabilization. Overall, this study provided new insights into the aggregation behavior of NPs in aquatic systems, which have significant implications for predicting the transport and fate of NPs in complex real-world environments.

1. Introduction

The large-scale production and commercial application of plastics result in the excess release of plastics into the aquatic environments, constituting up to 60–80% of marine litter (Alimi et al., 2018; Eerkes--Medrano et al., 2015; Erni-Cassola et al., 2017). These plastic wastes can be fragmented into nanoplastics (NPs) through chemical degradation, biodegradation, photo-degradation, thermal degradation, and mechanical abrasion (Alimi et al., 2018; Mao et al., 2018; Mao et al., 2020a; Mao et al., 2020b; Wu et al., 2019a). Besides, the use of primary NPs in personal care products, industrial abrades and medical fields has also accelerated their widespread pollution in environments (Alimi et al., 2018; Shams et al., 2020; Xu et al., 2022). Most of the concern has focused on the potential risks of NPs to ecosystems and human health (Gigault et al., 2021; Mitrano et al., 2021). The release of NPs into aquatic environments can result in toxicities such as cytotoxicity and metabolic disorders to a wide range of aquatic organisms including mammals (Besseling et al., 2015), fish (Alomar and Deudero 2017; Brun et al., 2019; Gu et al., 2020), zooplankton (Cole et al., 2016), and phytoplankton (Mao et al., 2018). The transport, bioavailability, and toxicity of NPs are tightly associated with their stability and aggregation behavior (Alimi et al., 2018). A thorough understanding of the stability and aggregation behavior of NPs in aquatic environments is important to reveal and predict their potential ecological effects.

Recently, the colloidal stability and aggregation behavior of NPs have been widely investigated in actual and simulated water (Liu et al., 2019; Liu et al., 2020; Mao et al., 2020b; Shams et al., 2020; Xu et al., 2021). Previous studies investigated the influence of water chemistry (i.

* Corresponding author.
E-mail address: gliu@rcees.ac.cn (G. Liu).

https://doi.org/10.1016/j.watres.2022.119313
Received 2 July 2022; Received in revised form 12 October 2022; Accepted 29 October 2022
Available online 31 October 2022

e., pH, ionic strength and valence), natural organic matter (NOM) and aging on the stability of polystyrene nanoplastics (PS NPs) in aqueous systems (Dong et al., 2020; Li et al., 2021a; Li et al., 2021b; Liu et al., 2019; Liu et al., 2020; Mao et al., 2020b; Shams et al., 2020). Usually, decreased pH and enhanced ionic strength promote the aggregation of PS NPs, and divalent cations (e.g., Ca^{2+} and Mg^{2+}) are more efficient to destabilize PS NPs than monovalent cations (Wang et al., 2021; Yu et al., 2019). Natural organic matter (NOM) is ubiquitously present in the aquatic environment, comprised of heterogeneous organic compounds such as humic acids (HA), excreted microbial products, proteins and polysaccharides (Junaid and Wang 2021). The interaction of NPs with NOM can lead to the development of diverse organic coating on the surface of NPs, known as eco-corona (Wheeler et al., 2021), which can modify the physiochemical properties of NPs and subsequently change their stability (Junaid and Wang 2021). As representative components of NOM, HA and proteins are well studied to affect the aggregation behavior of NPs (Li et al., 2021a; Li et al., 2021b; Liu et al., 2020). HA was reported to enhance the stability of PS NPs in NaCl solution but reduce their stability in $CaCl_2$ solutions due to the contributions of steric repulsion and cation bridging (Liu et al., 2020; Wang et al., 2021; Yu et al., 2019). Li et al. reported that bovine serum albumin (BSA), a model protein, strongly enhanced the stability of PS NPs in both NaCl and $CaCl_2$ solutions due to the dominant role of steric repulsion (Li et al., 2021a; Li et al., 2021b). In contrast, Liu et al. concluded that BSA strongly destabilized PS NPs in $CaCl_2$ solutions caused by additional cation bridging (Liu et al., 2020). Environmental aging is another important factor influencing the aggregation behavior of NPs (Liu et al., 2019; Mao et al., 2020b; Xu et al., 2021). As reported, sunlight aging could enhance surface hydrophilicity and oxygen-containing functional groups of PS NPs, resulting in the enhanced stability of NPs in NaCl solution and decreased stability in $CaCl_2$ solutions (Liu et al., 2019; Mao et al., 2020b). Overall, these studies help us to understand the influence of various environmental factors on the stability of NPs, especially the effect of NOM and photoaging.

However, in real environments, the influence of NOM and photoaging on the stability of NPs may coexist. It is well known that the adsorption of NOM is important as it influences the aggregation kinetics of NPs, which is significantly controlled by the physicochemical properties of NPs (Alimi et al., 2018; Li et al., 2021a). Photoaging is a significant process affecting the surface characteristics of NPs, but whether this can affect the adsorption of NOM and subsequent stability of PS NPs remains unclear. In addition, NOM is also known to undergo photochemical transformation after sunlight radiation (Chu et al., 2016; Goslan et al., 2006; Zhou et al., 2017). For example, due to its capacity to react with photons and reactive oxygen species (ROS), NOM could inhibit the photo-oxidation of organic pollutants in water (Guerard et al., 2009; Xu et al., 2011). NOM can also promote photo-degradation of pollutants due to the formation of the excited triplet state of DOM (3DOM*) and ROS (Zhang et al., 2022; Zhang et al., 2018). Notably, sunlight radiation was also reported to induce the crosslinking and assembly of protein-containing NOM, which was important for the formation of marine snow (micro- and macro-gels derived from biopolymers) in aquatic systems (Sun et al., 2019; Sun et al., 2017). Through interfering with the photoaging of NPs or through photochemical transformation, the adsorbed NOM may affect the aggregation behavior of NPs. Overall, in complex aquatic environments, photoaging and NOM are likely to have a combined effect on the stability of NPs. Although the independent influences of NOM and photoaging on the stability of NPs have been well investigated, the question remains whether and how NOM affects the stability of photoaged NPs and whether photoaging affects the stability of NPs in the presence of NOM. To better understand and predict the environmental behavior and fate of NPs in real aquatic environments, further studies regarding the combined effects of photoaging and NOM on the colloidal stability of NPs are needed.

This study aims to investigate the effects of NOM on the stability of photoaged NPs and the effects of photoaging on the stability of NOM-associated NPs. For relevant comparison, manufactured PS NPs commonly used in previous studies were used as the model NPs (Liu et al., 2019; Liu et al., 2020). First, PS NPs were aged under simulated light to investigate the effect of photoaging on the physicochemical properties and colloidal stability of PS NPs. Second, HA and BSA were selected as model NOM to study their interaction with pristine/aged PS NPs and their effects on the aggregation kinetics of PS NPs. Third, the influences of photoaging on the stability of PS NPs in the presence of HA or BSA were studied.

2. Materials and methods

2.1. Materials

A PS stock solution (aqueous suspension) with a concentration of 2.5% w/v (i.e., 25 g/L) was purchased from Macklin Biochemical Co., Ltd (Shanghai, China). According to the manufacturer, the diameter of PS NPs was 0.05–0.1 μm and there was no surface modification. Before the experiments, the PS suspension was diluted with ultrapure water to obtain 20 mg/L PS NPs and stored at 4–8 °C. The final concentration used in all experiments was 10 mg/L, which was considered as a representative NP concentration commonly used in aggregation kinetics studies (Liu et al., 2019; Liu et al., 2020; Wang et al., 2021; Yu et al., 2019). HA and BSA were purchased from Sigma-Aldrich (Shanghai, China) and used as a representative aquatic humic substances and proteins. The HA and BSA powders (1 g) were dissolved in 500 mL of ultrapure water and stirred for 24 h in the dark. The stock solution was then filtered through 0.22 μm Whatman membrane filters to get dissolved HA and BSA. The concentrations of stock HA and BSA were determined using a total organic content (TOC) analyzer. The concentrations of HA and BSA used in the experiment were 2 mg C/L, which was within the range of NOM concentrations found in natural aquatic environments and also commonly used in previous studies (Liu et al., 2020; Qu et al., 2010a; Shams et al., 2020). The electrolyte stock solutions were prepared by dissolving ACS-grade monovalent (NaCl) or divalent ($CaCl_2$) salts in ultrapure water and filtered through 0.22 μm filters. The electrolyte solutions were later diluted to desired concentrations to cover a wide range of environmental conditions. All solution pH in this study was adjusted to 6.5 using HCl and NaOH.

2.2. Radiation experiments

The aging experiments were conducted as described in previous studies (Liu et al., 2019; Qu et al., 2010a). The pristine PS NPs with a concentration of 20 mg/L (50 mL) was added into a 70 mL transparent quartz tube. The quartz tube was set in a photochemical reaction reactor with a magnetic stirrer and irradiated with a UV lamp (365 ± 50 nm), which provided approximately 2 mW/cm^2 of light intensity at the center of the reactor. To simulate the aging of PS NPs in the presence of NOM, the pristine PS NPs (20 mg/L) with HA or BSA (4 mg C/L) were prepared and aged under the same conditions. The aging time was set at 0, 6, 12, and 24 h, respectively. The harvest aged PS suspensions with and without HA/BSA were transferred into 100 mL glass bottles and blown with nitrogen, and the pH was adjusted to 6.5 with HCl and NaOH. Nitrogen was blown to keep pH stable and not affected by carbon dioxide in the air.

2.3. Characterization

A Zetasizer Nano ZS100 (Malvern Instruments, UK) was used to characterize the hydrodynamic size and zeta potential of PS NPs. The instrument was operated with a HeNe laser at a wavelength of 633 nm and a scattering angle of 90° The refractive and absorption indexes for PS NPs were 1.59 and 0.01, respectively. Scanning electron microscopy (SEM) was used to observe the morphology and conformation of selected

samples. The structural properties and surface functional groups of pristine and aged PS NPs, HA and BSA samples were characterized by attenuated total reflectance Fourier transform infrared spectroscopy (ATR-FTIR) and X-ray photoelectron spectroscopy (XPS) (Li et al., 2021a; Qu et al., 2016). ATR-FTIR and an FLS1400 fluorescence spectrofluorometer were further used to characterize the interaction between pristine/aged PS NPs and HA/BSA (Gu et al., 2015; Li et al., 2021a; Phong and Hur 2018). Detailed procedures of these characterization methods were presented in Text S2.

2.4. Aggregation kinetics measurements

The aggregation kinetics of PS NPs were measured with a time-resolved dynamic light scattering (DLS) technique using a Malvern Zetasizer instrument (Nano ZS, Malvern, UK) with a He–Ne laser at a wavelength of 633 nm and a fixed scattering angle of 90° (Xu et al., 2020). The pristine and aged PS NPs were sonicated in a water bath for 15 min before each measurement. For the aggregation kinetics of PS NPs without the presence of HA or BSA, 1 mL of the PS suspension was added to a 1 cm quartz cuvette, followed by adding 1 mL of the prepared NaCl or $CaCl_2$ solution. For the aggregation kinetics in the presence of HA and BSA, the PS NPs, HA or BSA and salt solution were mixed in a certain proportion, and the final concentrations of PS NPs and HA/BSA were 10 mg/L and 2 mg C/L, respectively. The aggregation kinetics were determined by detecting the hydrodynamic size change at a given time. The hydrodynamic size of PS NPs was continuously monitored every 30 s for 30 min and all measurements were conducted in triplicate (Ter Halle et al. 2017).

Detailed aggregation kinetic calculation can be found in the Supporting Information (Text S1). The attachment efficiency (α) was calculated to characterize the aggregation capacity of PS NPs in salt solutions with different concentrations, which increased with the increase in salt concentration. The salt concentration when α reaches its maximum ($\alpha = 1$) was called the critical coagulation concentration (CCC), which was used to determine the aggregation potential of PS NPs (Mao et al., 2020b; Xu et al., 2021). The concentration was first chosen as 100, 200, 300, 400, 500, 600, 700, 800, 900, and 1000 mM for NaCl and 10, 20 30, 40, and 50 mM for $CaCl_2$ to get general aggregation kinetics of PS NPs with and without NOM, and evaluate the approximate range of their CCC values. If these salt concentrations are insufficient to obtain an exact CCC value, additional salt concentrations around the CCC value are added. The effect of NOM on the stability of PS NPs was evaluated by calculating the ratio of the CCC value of PS NPs with NOM and that of individual PS NPs (Text S1). Due to the strong stability of pristine/aged PS NPs in the presence of NOM, it is sometimes impossible to determine their CCC values. The ratio of the aggregation rate of PS NPs with NOM and that of individual PS NPs (β) at a given salt concentration was calculated to evaluate the inhibition ($\beta < 1$) or promotion ($\beta > 1$) efficiency of NOM on the aggregation of pristine/aged PS NPs.

3. Results and discussions

3.1. Characterizations of PS NPs before and after photoaging

The SEM images showed that the pristine PS NPs exhibited a regular spherical morphology with an average diameter of about 70 nm, and there was no significant difference in the shape and size of PS NPs after aging (Fig. S1). The average hydrodynamic size of pristine PS NPs was 113.5 ± 4.2 nm, which decreased slightly after aging (Table S1). The zeta potential was −40.1 ± 1.7 mV in ultrapure water (Fig. S2 and S3), suggesting high stability of PS NPs (Liu et al., 2019; Liu et al., 2020). For the photoaged PS NPs, its absolute value of zeta potential was hardly altered in NaCl solution, while it decreased significantly in $CaCl_2$ solution (Fig. S2a and S2b). For pristine PS NPs, the adsorption peaks at 698 and 831 cm^{-1} were attributed to the aromatic C–H bending (Luo et al., 2019), and the C = C stretching of the aromatic ring and alkene at 1494 and 1603 cm^{-1} were also identified (Fig. S2c) (Liu et al., 2019; Mao et al., 2020b). The spectra of aged PS NPs showed a broad adsorption peak at 1600–1755 cm^{-1} and 3200–3500 cm^{-1} of C = O and O–H stretching (Fig. S2c), indicating the presence of O-containing functional groups, e.g. hydroxyl and carboxyl groups (Xu et al., 2021). After photoaging, the hydrophilic functional groups associated with PS NPs increased due to their higher polarity indexes (Fig. S2e, Table S2) (Lian et al., 2019; Liu et al., 2019). Besides, the results also suggested that HA was rich in O-containing functional groups, while BSA was rich in amino groups (Fig. S2d and S2f).

3.2. Aggregation kinetics of photoaged ps NPs

As shown in Fig. 1, CCC values of PS NPs increased with extended aging time in NaCl solutions, implying that aging enhanced the colloidal stability of PS NPs in the presence of NaCl (Liu et al., 2019). Considering there was no significant change in zeta potential after photoaging (Fig. S2a), such differences in aggregation behavior of aged PS NPs were unlikely caused by electrostatic interaction. It was noticed that light radiation induced O-containing hydrophilic functional groups after aging (Fig. S2c and S2e), which may inhibit the aggregation of NPs due to the enhanced hydration repulsion (Ou et al., 2021; Qu et al., 2010b). In contrast to the case in NaCl solution, the photoaging decreased the CCC values of aged PS NPs in $CaCl_2$ solution (Fig. 1b). As previously reported, Ca^{2+} could bind with O-containing functional groups on the aged PS surface, resulting in strong charge neutralization and cation bridging between aged PS NPs (Fig. S2b) (Liu et al., 2019; Mao et al., 2020b; Shams et al., 2020). Thus, the aged PS NPs had less negative potentials than pristine PS NPs in $CaCl_2$ solution, which lead to the decrease of their colloidal stability. A similar observation was reported by Wang et al. in their study of biochar colloids, where they found that HNO_3 aging promoted the aggregation behavior because of the high binding efficiency of Ca^{2+} with the carboxyl groups on aged biochar surface (Wang et al., 2019).

3.3. Effect of HA on the aggregation kinetics of photoaged PS NPs

The presence of 2 mg/L HA greatly enhanced the stability of PS NPs in NaCl solutions (Fig. 2a and S9). Although negatively charged, HA can readily adsorb onto PS NPs by hydrophobic and π-π interaction (Liu et al., 2020; Xu et al., 2021). As previously reported, the adsorbed HA molecules could produce additional steric repulsion between PS NPs, inhibiting their aggregation behavior (Liu et al., 2020; Shams et al., 2020). Differently, the CCC values of aged PS NPs in $CaCl_2$ solutions in the presence of HA were lower than that of pristine PS NPs (8 mM vs. 38 mM $CaCl_2$), implying that HA significantly increased the aggregation of PS NPs in $CaCl_2$ solutions (Fig. 2b and S9). HA contained abundant negatively charged O-containing functional groups like carboxyl and hydroxyl groups (Fig. S2d). These moieties can complex with Ca^{2+} and form molecular bridging between PS NPs and thus strongly destabilize PS NPs (Liu et al., 2020; Wang et al., 2021; Wu et al., 2019b).

The aging of PS NPs may affect the interaction between PS NPs and HA. As shown in Fig. 2a, HA inhibited the aggregation of PS NPs in NaCl solutions, but the degree of inhibition varied between pristine and aged PS NPs. In the presence of HA, the attachment efficiencies of photoaged PS NPs seemed to be higher than that of pristine PS NPs (Fig. 2a). Because of the strong stability of pristine and aged PS NPs in the presence of HA, the CCC values of them were not determined. With the increase in aging time from 0 h to 24 h, the β value of PS NPs in the presence of HA increased from 0.068 to 0.193 in 400 mM NaCl solution (Text S1, Fig. S13), suggesting that the inhibiting effect of HA was much weakened after the aging of PS NPs. The zeta potential of pristine and aged PS NPs did not change notably after equilibrating with 2 mg/L HA (Fig. S4), implying that electrostatic interaction was not responsible for the decrease in inhibition efficiency. Pristine PS NPs were rich in aromatic components (Fig. S2c), which were conducive to the adsorption or

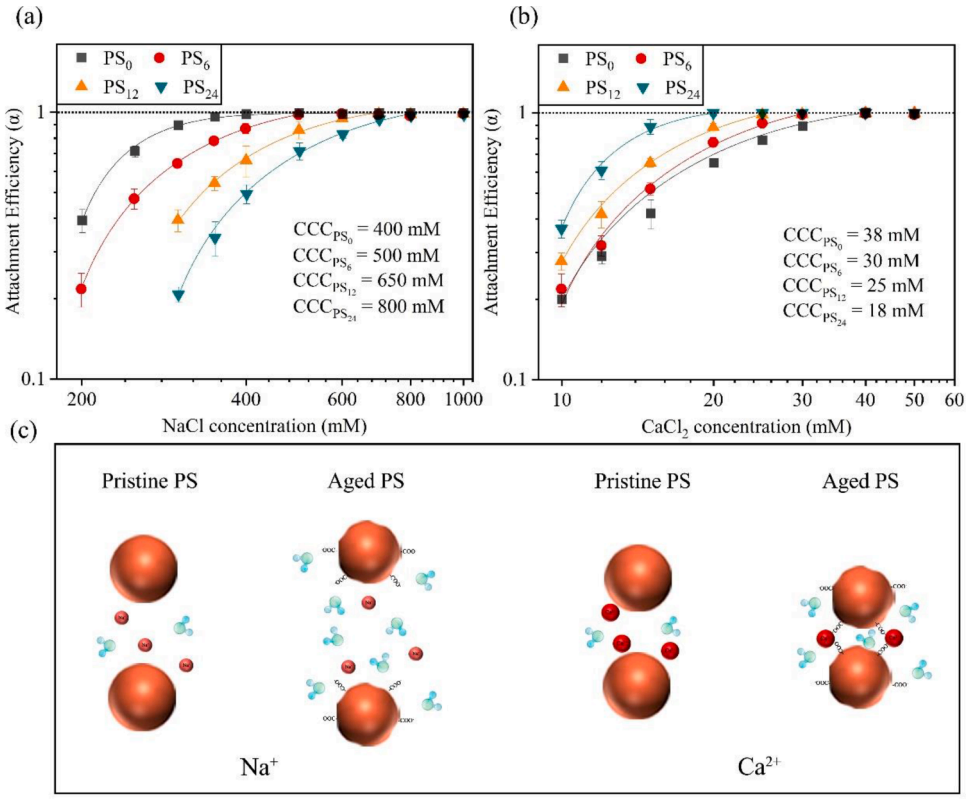

Fig. 1. The aggregation kinetics of pristine and aged PS NPs in NaCl (a) and $CaCl_2$ (b) solutions; Schematic diagram of the effect of photoaging on the stability of PS NPs (c). Subscripts 0, 6, 12 and 24 mean aging times of 0, 6, 12 and 24 h.

hetero-aggregation of HA through π-π interaction and hydrophobic force (Liu et al., 2020; Xu et al., 2021). The aromatic components decreased and O-containing functional groups increased after the aging of PS NPs (Fig. S2c and S2e) (Liu et al., 2019; Xu et al., 2021), and this might decrease the adsorption of HA due to reduced π-π interaction and hydrophobic force (Xu et al., 2021). Based on DLS analysis, pristine PS NPs seemed to adsorb more HA than aged PS NPs as revealed by the difference of the mean hydrodynamic diameter PS NPs before and after interaction with HA, but the difference was not significant (Table S1). SEM results also showed that the size and shape of PS NPs were not significantly different before and after HA adsorption (Fig. S1). Thus, it may be difficult to compare the adsorption of HA on pristine and aged PS NPs by particle size. The FTIR spectra of pristine PS NPs in the presence of HA was the result of superposition of PS NPs and HA alone (Fig. S2c, S2d and 2c), implying the adsorption and coverage of HA on PS NPs. The effect of HA on the spectra of aged PS NPs was smaller than that of pristine PS NPs (Fig. S2c and 2c), indicating that HA might be less absorbed on aged PS NPs. Notably, the FTIR is not a quantitative technique, but the results here were helpful to understand the interaction of PS NPs and NOM on a semi-quantitative level. Furthermore, the fluorescence spectra revealed that the fluorescence of aromatic C=C components of HA was quenched after the addition of PS NPs, but the fluorescence quenching degree was decreased to a certain extent when aged PS NPs were added (Fig. 2d). This indicated that the interaction between HA and PS NPs was weakened to some extent, and the steric repulsion caused by absorbed HA molecules decreased with the aging of PS NPs, thus reducing the inhibitory effect of HA on PS NPs aggregation in NaCl solutions (Fig. 2e).

Fig. 2b shows the effect of HA on the aggregation kinetics of photoaged PS NPs in $CaCl_2$ solutions. In the presence of HA, the CCC values of PS_0, PS_6, PS_{12} and PS_{24} were 8, 10, 12, 13 mM, respectively, lower than the CCC values of PS NPs alone at the corresponding time. It suggests that HA also promoted the aggregation of aged PS NPs in $CaCl_2$ solutions, which was attributed to the bridging effect of Ca^{2+} and HA molecules absorbed on PS surface, as described above. The ratios of CCC of PS NPs with HA and without HA were determined as 0.21, 0.33, 0.44, and 0.67 for PS_0, PS_6, PS_{12} and PS_{24}, respectively, suggesting that the promoting effect of HA on the aggregation of PS NPs was decreased after the aging of PS NPs. This was also confirmed by the decrease in the β value from 5.34 to 2.33 in 10 mM $CaCl_2$ solution as the aging time increased from 0 h to 24 h (Fig. S13). Similar to that in NaCl solutions, the weak interaction between HA and aged PS NPs decreased the molecular bridging with Ca^{2+} between HA-absorbed PS NPs, thus reducing the promoting effect of HA on PS NPs aggregation in $CaCl_2$ solutions (Fig. 2e). Qu et al. reported that HA had little influence on the stability of aged fullerene nanoparticles (nC_{60}) in NaCl and $CaCl_2$ solutions due to reduced adsorption on UV-irradiated nC_{60} surface (Qu et al., 2010a). Our previous study also suggested that the effect of dissolved black carbon on the stability of PS NPs was weakened after the aging of PS NPs (Xu et al., 2021).

3.4. *Effect of BSA on the aggregation kinetics of photoaged PS NPs*

As shown in Fig. S3a and S10, the presence of 2 mg/L BSA strongly inhibited the aggregation of PS NPs in NaCl solutions and its stabilization effect on PS NPs was larger than that of HA. Unlike HA, the absolute value of the zeta potential of PS NPs in the presence of BSA was lower than that of PS NPs without BSA (Fig. S3) due to the strong interaction between BSA and PS NPs screened surface charges of PS NPs (Li et al., 2021a; Liu et al., 2020). Therefore, steric repulsion rather than electrostatic interaction determined the aggregation behavior of PS NPs in the presence of BSA (Dong et al., 2020; Kihara et al., 2019; Li et al., 2021a; Liu et al., 2020). Liu et al. also reported a similar result, that strong hydrophobic interaction contributed to the formation of protein corona on PS NPs, enhancing their colloidal stability in NaCl solutions (Liu et al., 2020). They further found that BSA could promote the

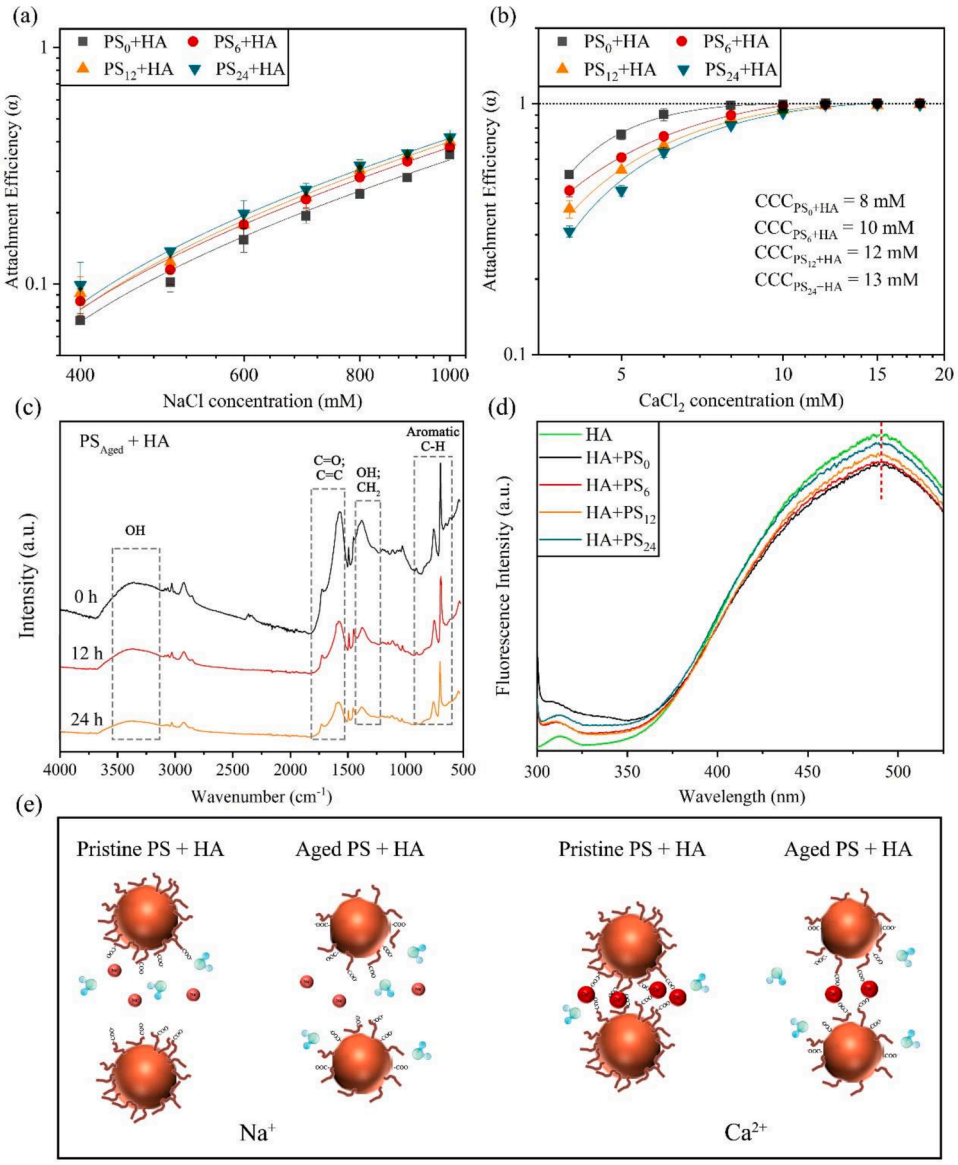

Fig. 2. Influence of HA on the aggregation kinetics of pristine and aged PS NPs in NaCl (a) and $CaCl_2$ (b) solutions; Characterization of the interaction between HA and PS NPs with FTIR (a) and fluorescence spectra (b); Schematic diagram of the effect of HA on the stability of pristine/aged PS NPs (e). Subscripts 0, 6, 12 and 24 mean aging times of 0, 6, 12 and 24 h.

aggregation of PS NPs in $CaCl_2$ solutions due to the role of cation bridging (Liu et al., 2020). However, both our study and other publications showed that BSA increased the stability of PS NPs in $CaCl_2$ solutions because of the dominant role of steric repulsion (Li et al., 2021a; Li et al., 2021b). Such a difference may be attributed to different characteristics of PS NPs and BSA such as particle size, surface functional groups and chemical composition.

As can be seen from Fig. 3a, the addition of BSA also decreased the aggregation attachment efficiency of aged PS NPs in NaCl solutions, but there was no significant difference between different aging times. The β value decreased from 0.34 to 0.13 in 100 mM NaCl solution after the aging of PS NPs (Fig. S13), implying that the effect of BSA on the stability of PS NPs was stronger. Notably, the aggregation efficiency of PS NPs in the presence of BSA decreased with increasing aging time of PS NPs in $CaCl_2$ solutions (Fig. 3b), accordingly, the β values of PS_0, PS_6, PS_{12} and PS_{24} in 10 mM $CaCl_2$ solution were 0.86, 0.52, 0.24 and 0.07, respectively (Fig. S13), which indicated that BSA had a stronger inhibitory effect on aged PS NPs in $CaCl_2$ solutions. Thus the higher stability of photoaged PS NPs in the presence of BSA might be attributed to the fact that the protein corona structure provided more steric repulsion for aged PS NPs than pristine PS NPs.

Analyzed from FTIR and XPS results, BSA contained abundant positively charged amide groups (Fig. S2d and S2f), which could bind more easily with O-containing groups on aged PS NPs via hydrogen bonding and electrostatic attraction.(Contreras et al., 2011) Thus, in the presence of BSA, the absolute value of the zeta potential of PS NPs decreased with increasing aging time (Fig. S3), indicating that the interaction between BSA and PS NPs was enhanced. Compared with pristine PS NPs, the FTIR spectra of aged PS NPs with BSA added were closer to that of BSA alone (Fig. S2c and 3c), which suggests that aged PS NPs adsorbed more BSA. Moreover, fluorescence spectra showed that tyrosin and/or tryptophan and/or phenylalanine fluorescence of BSA was quenched due to the interaction with PS NPs (Fig. 3d), and there was a strong complexation between PS NPs and the amino acid residues of BSA (Li et al., 2021a). As the aging time increased, the corresponding fluorescence intensity of BSA reduced (Fig. 3d), implying stronger interaction between BSA and photoaged PS NPs. Additionally, the SEM images also showed that PS_{24} seemed to adsorb more BSA than PS_0

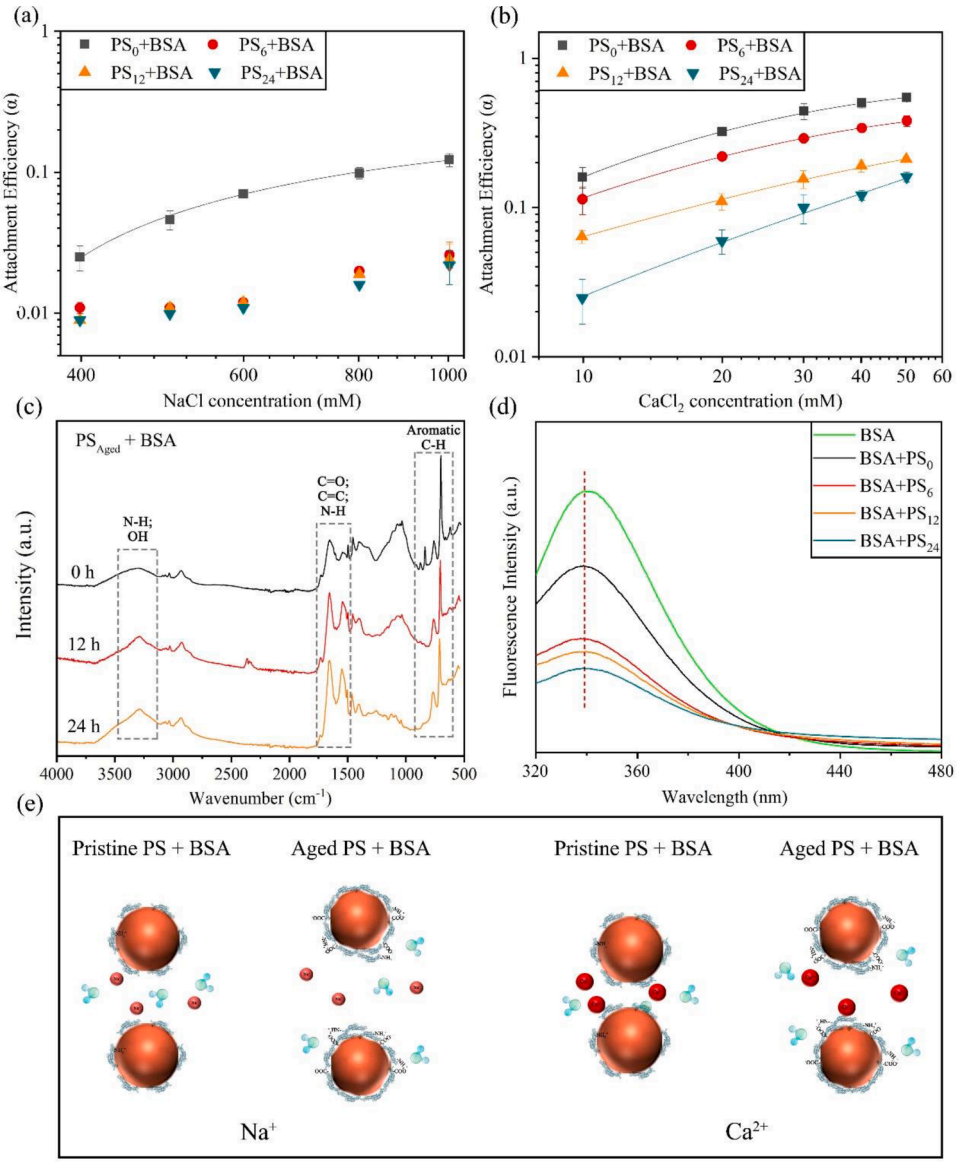

Fig. 3. Influence of BSA on the aggregation kinetics of pristine and aged PS NPs in NaCl (a) and $CaCl_2$ (b) solutions; Characterization of the interaction between BSA and PS NPs with FTIR (a) and fluorescence spectra (b). Schematic diagram of the effect of BSA on the stability of pristine/aged PS NPs (e). Subscripts 0, 6, 12 and 24 mean aging times of 0, 6, 12 and 24 h.

(Fig. S1), and this may explain why aged PS NPs had higher stability than pristine PS NPs in both NaCl and $CaCl_2$ solutions (Fig. 3e).

Similar results were reported in membrane fouling research, which stated that pre-ozonation significantly alleviated membrane fouling caused by HA but aggravated BSA fouling (Cheng et al., 2016; Levitsky et al., 2011). Although no more detailed explanation was given in this study, we propose that the hydrophobic and π-π interaction controlled the adsorption of HA on pristine/aged surfaces and hydrogen bonding and electrostatic attraction were dominant forces between BSA and pristine/aged surfaces. The distinct interaction of HA and BSA with PS NPs resulted in their distinct effects on the colloidal stability of PS NPs. Unlike the adsorption of HA to PS NPs through hydrophobic and π-π interactions, the interaction between BSA and PS NPs was mainly dominated by electrostatic attraction and hydrogen bonding rather than hydrophobic interaction, thus the steric repulsion generated by absorption of BSA molecules between aged PS NPs was greater than that between pristine PS NPs. Sun et al. suggested that although aged graphene oxide (GO) was more hydrophobic than GO which contained more O-containing functional groups, the interaction between BSA and aged GO was weaker than that of pristine GO, and thus they found that the thinner BSA coating on aged GO resulted in the less stability compared to pristine GO (Sun et al., 2021a). A recent study also reported that PS-COOH interacted more efficiently with amino acid residues of BSA than PS-Bare, so higher CCCs for PS-COOH in the presence of BSA than in the case of PS-Bare were observed (Li et al., 2021a).

3.5. *Effect of photoaging on the stability of PS NPs with HA*

Fig. 4a shows the influence of photoaging on the aggregation kinetics of PS NPs with 2 mg/L HA in NaCl solutions. With the increase in aging time, the aggregation attachment efficiency of PS NPs with HA increased in NaCl solutions (Fig. 4a and S11), which indicated that aging decreased the stability of PS NPs with HA. The increase in β values from 0.07 to 0.61 when the aging time increased from 0 h to 24 h in 400 mM NaCl solution suggests that the inhibitory effect of HA on the aggregation of PS NPs was decreased after light radiation. There was a slight decrease in the absolute value of the zeta potential of PS NPs with HA (Fig. S6), and thus electrostatic interaction could partly explain the

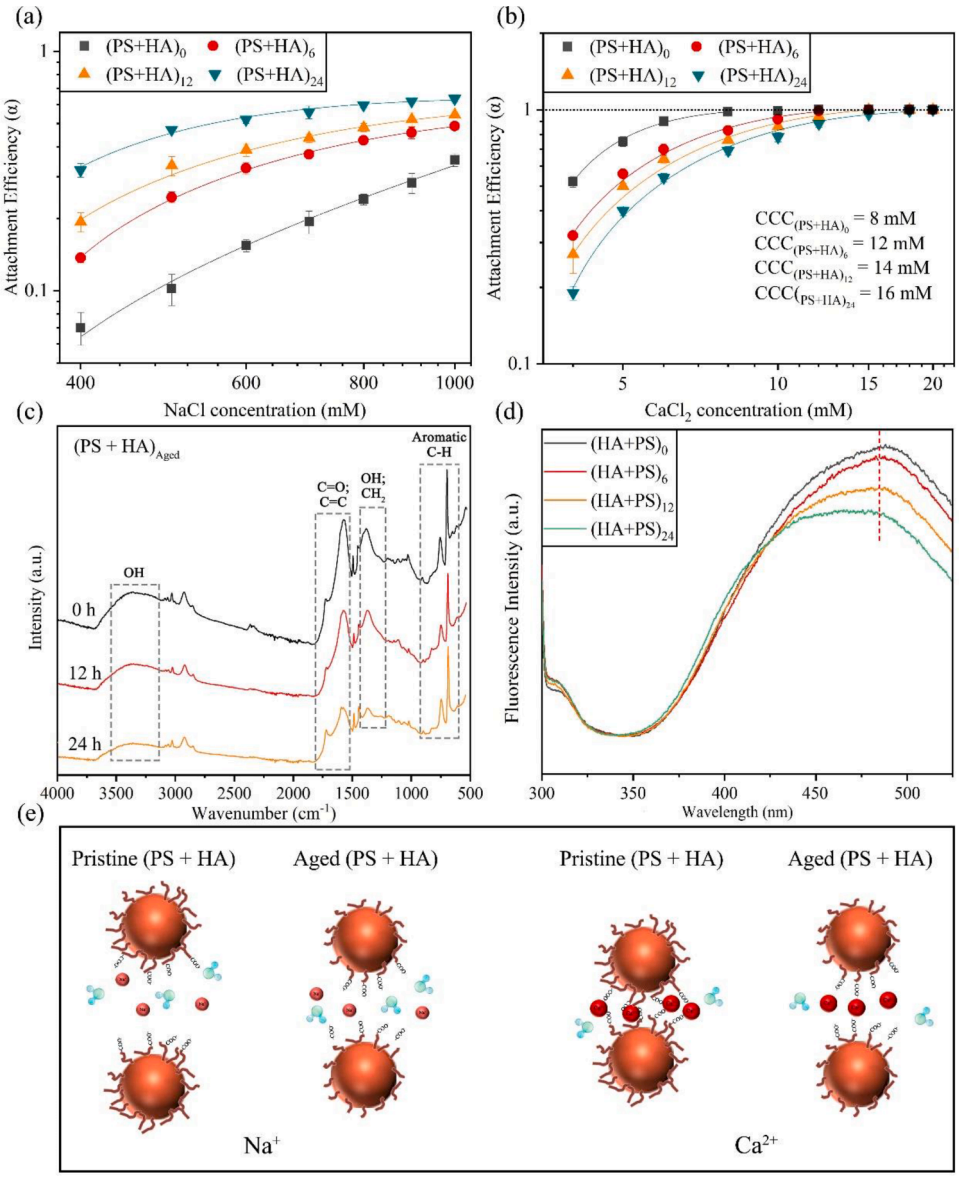

Fig. 4. The effect of photoaging on the aggregation kinetics of PS NPs with HA in NaCl (a) and $CaCl_2$ (b) solutions; The FTIR (c) and fluorescence (d) spectra of PS NPs with HA; Schematic diagram of the effect of photoaging on the stability of HA associated PS NPs (e). Subscripts 0, 6, 12 and 24 mean aging times of 0, 6, 12 and 24 h.

enhanced aggregation. According to the FTIR spectra of PS NPs and HA complexes, the functional groups of PS NPs changed little but the intensity of HA functional groups decreased after aging (Fig. 4c), implying HA might be more easily oxidized than PS NPs. Moreover, the fluorescence of aromatic components of HA was quenched after light radiation, and the quenching degree increased with the increase in aging time (Fig. 4d). This suggests that the reductive reactive components of HA might compete for photons with PS NPs, leading to degradation or disintegration of HA. A recent study reported that chromophores in HA and fulvic acids such as aromatic ketones, aldehydes, quinones, and phenolic compounds could reduce the photodegradation rates of PP MPs through acting as both reactive oxygen species (ROS) scavengers and optical light filters (Wu et al., 2021). Duan et al. also implied that carboxyl-coated PS NPs produced fewer ROS than bare PS NPs due to coating scavenging (Duan et al., 2022). Thus, HA was likely to compete for photons and ROS, and underwent photo-degradation. Although the observed results could be partially explained by the aging of PS NPs and decreased interaction between HA and PS NPs, more importantly, we propose that the destruction or reconstruction of the HA coating and the reduction of steric repulsion might be the main reason for the less stability of PS NPs with HA in NaCl solutions after aging (Fig. 4e).

On the contrary, the CCCs of PS NPs with HA increased from 8 mM to 11, 14 and 16 mM in $CaCl_2$ solutions when the aging time increased from 0 h to 6, 12, and 24 h, respectively (Fig. 4b), which indicated that photoaging enhanced the stability of PS NPs with HA. As mentioned above, the Ca^{2+} bridging with HA coating was a dominant factor promoting the aggregation of PS NPs (Fig. 2b). Thus the higher stability of PS NPs with HA in $CaCl_2$ solutions after aging was attributed to the destruction of HA coating and less bridging effect (Fig. 4e).

3.6. *Effect of photoaging on the stability of PS NPs with BSA*

Fig. 5a shows the shift in the hydrodynamic size of PS NPs with BSA as a function of time at the different aging times. With the aging time increasing from 0 h to 6 h, the particle size of PS NPs increased from 100 nm to nearly 500 nm (Fig. 5a). Significantly, long-time radiation (12 h and 24 h) lead to the formation of large particles (Fig. S14 and S15), which suggests that the light radiation strongly enhanced the

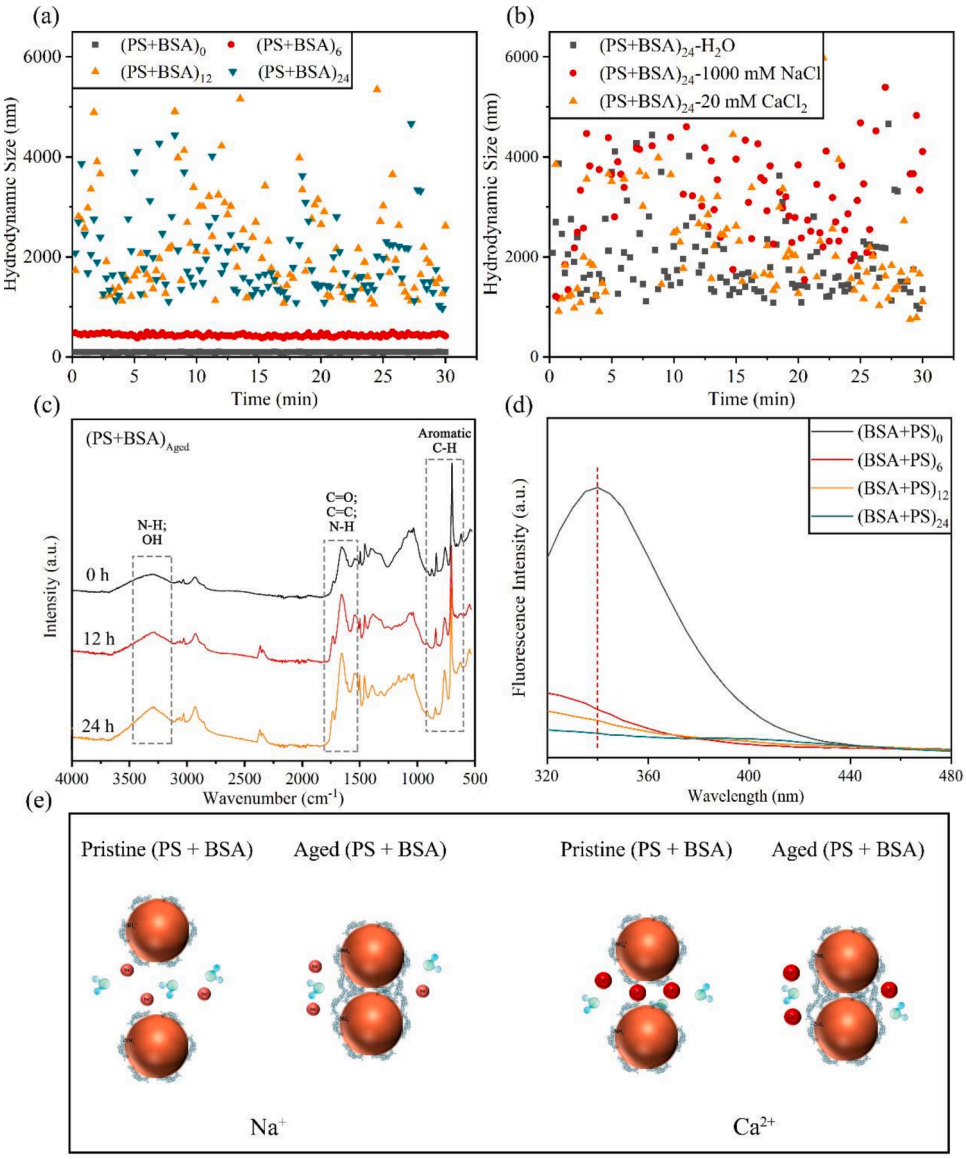

Fig. 5. The effect of photoaging on the aggregation kinetics of PS NPs with BSA in NaCl (a) and $CaCl_2$ (b) solutions; The FTIR (c) and fluorescence (d) spectra of PS NPs with BSA; Schematic diagram of the effect of photoaging on the stability of BSA associated PS NPs (e). Subscripts 0, 6, 12 and 24 mean aging times of 0, 6, 12 and 24 h.

aggregation of PS NPs in the presence of BSA. The FTIR spectra showed that more amino groups of BSA occurred while the functional groups of PS NPs hardly changed after photoaging (Fig. 5c), which indicated that more BSA covered the surface of PS NPs. The fluorescence spectra showed that tyrosin and/or tryptophan and/or phenylalanine fluorescence of BSA was significantly quenched after light radiation (Fig. 5d), implying that the aging process induced the denaturation of BSA molecules. Most studies reported that sunlight radiation could result in aggregation or assembly of BSA, protein-containing dissolved organic matter (DOM) and extracellular polymeric substances (EPS) in water bodies via chemical crosslinking (Sun et al., 2019; Sun et al., 2021b; Sun et al., 2017). Similarly, we also found the hydrodynamic size of a single BSA (2 mg/L) was 550 ± 196 nm after 24 h light radiation (Fig. S15), confirming the photo-flocculation of BSA molecules. Notably, the hydrodynamic size of PSs with BSA was much larger than that of single BSA at the same aging time, so the large aggregate was the complex of PS NPs and BSA flocculates, which was further confirmed by the SEM images (Fig. S1). Therefore, due to the strong interaction between PS NPs and BSA, the BSA molecules bridged and wrapped PS NPs, promoting the formation of large aggregates and destroying the stability of PS NPs under radiation (Fig. 5a, 5b and 5e). Meanwhile, neither the salt concentration nor ionic type affected the further aggregation of PS NPs in salt solutions (Fig. 5b and S16). On the one hand, the hetero-aggregation of PS NPs and flocculated BSA induced high coverage of BSA layer, which might enhance the stability of hetero-aggregates due to steric repulsion. On the other hand, colloidal forces had a negligible effect on the aggregation state of the formed large hetero-aggregates due to the diffusion limitation (Xu et al., 2021; Xu et al., 2020).

4. Conclusions and environmental implications

This study systematically investigated the interaction mechanisms of HA/BSA and aged/pristine NPs, the photoaging of NPs with and without HA/BSA, as well as further effect on the stability of NPs, providing new insights into the stability of NPs in complex aquatic environments. The most important results are that after the aging of PS NPs, the effect of HA on the stability of PS NPs was weakened while the inhibitory effect of BSA on the aggregation kinetics of PS NPs was enhanced with aging

time. In addition, the high or low stability of PS NPs in the presence of HA in NaCl or $CaCl_2$ solutions was disrupted by light radiation, while the stability of PS NPs with BSA was destroyed due to the photo-flocculation of BSA molecules.

Beyond this, this study also has important implications for other topics. The adsorption of NOM to the surface of nanoparticles, known as eco-corona formation, can modify the surface properties of the nanoparticles and subsequently affect their transport, fate and ecological toxicity in environments (Wheeler et al., 2021). However, few studies paid attention to the formation mechanisms and evolution of eco-corona under environmental conditions. The present study showed that the formation of eco-corona was mediated by multiple forces between NOM and NPs, mainly depending on the source of NOM and the aging degree of NPs. Generally, hydrophobic and π-π interaction controlled the formation of HA-derived corona on surface of PS NPs while hydrogen bonding and electrostatic attraction were dominant in protein-corona development. Moreover, the formed eco-corona was also changeable: photoaging may induce the destruction of HA-corona and the photo-flocculation of protein-corona. The formation and evolution of eco-corona significantly affect the stability of NPs. NOM, especially microbial derived-polymers, can nucleate and form large flocs called marine snow after a series of physiochemical processes like homo- and hetero-aggregation (Quigg et al., 2021). Marine snow took part in many biogeochemical cycles in aquatic environments, and it was also reported to enhance the sinking of MPs and their bioavailability to benthic organisms (Porter et al., 2018). Notably, studies reported that light-induced aggregation of protein-containing NOM and EPS in aquatic environments was related to marine snow formation (Sun et al., 2019; Sun et al., 2017). Learned from this study, NPs significantly promoted cross-linked BSA to form larger flocs than BSA alone. Therefore, MPs and NPs may take part in the photo-flocculation of protein-containing NOM to form marine snow, which may further affect processes such as aggregation and sedimentation as well as biological risks in aquatic systems.

Supporting Information

The aggregation kinetics of PS NPs (Text S1); Sample characterization (Text S2); The SEM images of prepared samples (Fig. S1); The characterization of the zeta potential (Fig. S2-S5); The hydrodynamic size of pristine/aged PS NPs in ultrapure water before and after interaction with NOM (Table S1); The surface elemental concentration and the polarity indexes of samples (Table S2); Representative shift curves of hydrodynamic size of samples in ultrapure water and selected salt concentration (Fig. S7-S11); The aggregation rates of selected samples (Fig. S12); The β values of selected samples (Fig. S13); The photo-flocculation of BSA and BSA with PS NPs after aging (Fig. S14); The hydrodynamic size of BSA with and without PS NPs after photo-aging (Fig. S15); Effect of salt type on the hydrodynamic size of PS NPs with BSA after 6 h aging (Fig. S16).

Declaration of Competing Interest

The authors declare that they have no known competing financial interests or personal relationships that could have appeared to influence the work reported in this paper.

Data availability

Data will be made available on request.

Acknowledgments

The present work has been financially supported by the National Key R&D Program of China (2018YFE0204100).

Supplementary materials

Supplementary material associated with this article can be found, in the online version, at doi:10.1016/j.watres.2022.119313.

References

Alimi, O.S., Farner Budarz, J., Hernandez, L.M., Tufenkji, N., 2018. Microplastics and nanoplastics in aquatic environments: aggregation, deposition, and enhanced contaminant transport. Environ. Sci. Technol. 52 (4), 1704–1724.
Alomar, C., Deudero, S., 2017. Evidence of microplastic ingestion in the shark Galeus melastomus Rafinesque, 1810 in the continental shelf off the western Mediterranean Sea. Environ. Pollut. 223, 223–229.
Besseling, E., Foekema, E.M., Van Franeker, J.A., Leopold, M.F., Kuhn, S., Bravo Rebolledo, E.L., Hesse, E., Mielke, L., Ijzer, J., Kamminga, P., Koelmans, A.A, 2015. Microplastic in a macro filter feeder: humpback whale Megaptera novaeangliae. Mar. Pollut. Bull. 95 (1), 248–252.
Brun, N.R., van Hage, P., Hunting, E.R., Haramis, A.G., Vink, S.C., Vijver, M.G., Schaaf, M.J.M., Tudorache, C., 2019. Polystyrene nanoplastics disrupt glucose metabolism and cortisol levels with a possible link to behavioural changes in larval zebrafish. Commun. Biol. 2, 382.
Cheng, X., Liang, H., Ding, A., Qu, F., Shao, S., Liu, B., Wang, H., Wu, D., Li, G., 2016. Effects of pre-ozonation on the ultrafiltration of different natural organic matter (NOM) fractions: membrane fouling mitigation, prediction and mechanism. J. Memb. Sci. 505, 15–25.
Chu, C., Erickson, P.R., Lundeen, R.A., Stamatelatos, D., Alaimo, P.J., Latch, D.E., McNeill, K., 2016. Photochemical and nonphotochemical transformations of cysteine with dissolved organic matter. Environ. Sci. Technol. 50 (12), 6363–6373.
Cole, M., Lindeque, P.K., Fileman, E., Clark, J., Lewis, C., Halsband, C., Galloway, T.S., 2016. Microplastics alter the properties and sinking rates of zooplankton faecal pellets. Environ. Sci. Technol. 50 (6), 3239–3246.
Contreras, A.E., Steiner, Z., Miao, J., Kasher, R., Li, Q., 2011. Studying the role of common membrane surface functionalities on adsorption and cleaning of organic foulants using QCM-D. Environ. Sci. Technol. 45 (15), 6309–6315.
Dong, Z., Hou, Y., Han, W., Liu, M., Wang, J., Qiu, Y., 2020. Protein corona-mediated transport of nanoplastics in seawater-saturated porous media. Water Res. 182, 115978.
Duan, J., Li, Y., Gao, J., Cao, R., Shang, E., Zhang, W., 2022. ROS-mediated photoaging pathways of nano- and micro-plastic particles under UV irradiation. Water Res. 216, 118320.
Eerkes-Medrano, D., Thompson, R.C., Aldridge, D.C., 2015. Microplastics in freshwater systems: a review of the emerging threats, identification of knowledge gaps and prioritisation of research needs. Water Res. 75, 63–82.
Erni-Cassola, G., Gibson, M.I., Thompson, R.C., Christie-Oleza, J.A., 2017. Lost, but found with nile red: a novel method for detecting and quantifying small microplastics (1 mm to 20 um) in environmental samples. Environ. Sci. Technol. 51 (23), 13641–13648.
Gigault, J., El Hadri, H., Nguyen, B., Grassl, B., Rowenczyk, L., Tufenkji, N., Feng, S., Wiesner, M., 2021. Nanoplastics are neither microplastics nor engineered nanoparticles. Nat. Nanotechnol. 16 (5), 501–507.
Goslan, E.H., Gurses, F., Banks, J., Parsons, S.A., 2006. An investigation into reservoir NOM reduction by UV photolysis and advanced oxidation processes. Chemosphere 65 (7), 1113–1119.
Gu, W., Liu, S., Chen, L., Liu, Y., Gu, C., Ren, H.Q., Wu, B., 2020. Single-cell RNA sequencing reveals size-dependent effects of polystyrene microplastics on immune and secretory cell populations from zebrafish intestines. Environ. Sci. Technol. 54 (6), 3417–3427.
Gu, Y.L., Yin, M.X., Zhang, H.M., Wang, Y.Q., Shi, J.H., 2015. Study on the binding interaction of chromium(VI) with humic acid using UV-vis, fluorescence spectroscopy and molecular modeling. Spectrochim. Acta A Mol. Biomol. Spectrosc. 136 (Pt C), 1702–1709.
Guerard, J.J., Chin, Y.-P., Mash, H., Hadad, C.M., 2009. Photochemical fate of sulfadimethoxine in aquaculture waters. Environ. Sci. Technol. 43 (22), 8587–8592.
Junaid, M., Wang, J., 2021. Interaction of nanoplastics with extracellular polymeric substances (EPS) in the aquatic environment: a special reference to eco-corona formation and associated impacts. Water Res. 201, 117319.
Kihara, S., van der Heijden, N.J., Seal, C.K., Mata, J.P., Whitten, A.E., Koper, I., McGillivray, D.J., 2019. Soft and hard interactions between polystyrene nanoplastics and human serum albumin protein corona. Bioconjug. Chem. 30 (4), 1067–1076.
Levitsky, I., Duek, A., Arkhangelsky, E., Pinchev, D., Kadoshian, T., Shetrit, H., Naim, R., Gitis, V., 2011. Understanding the oxidative cleaning of UF membranes. J. Memb. Sci. 377 (1–2), 206–213.
Li, X., He, E., Jiang, K., Peijnenburg, W., Qiu, H., 2021a. The crucial role of a protein corona in determining the aggregation kinetics and colloidal stability of polystyrene nanoplastics. Water Res. 190, 116742.
Li, X., He, E., Xia, B., Liu, Y., Zhang, P., Cao, X., Zhao, L., Xu, X., Qiu, H., 2021b. Protein corona-induced aggregation of differently sized nanoplastics: impacts of protein type and concentration. Environmental Science: Nano 8 (6), 1560–1570.
Lian, F., Yu, W., Wang, Z., Xing, B., 2019. New Insights into black carbon nanoparticle-induced dispersibility of goethite colloids and configuration-dependent sorption for phenanthrene. Environ. Sci. Technol. 53 (2), 661–670.
Liu, Y., Hu, Y., Yang, C., Chen, C., Huang, W., Dang, Z., 2019. Aggregation kinetics of UV irradiated nanoplastics in aquatic environments. Water Res. 163, 114870.

Liu, Y., Huang, Z., Zhou, J., Tang, J., Yang, C., Chen, C., Huang, W., Dang, Z., 2020. Influence of environmental and biological macromolecules on aggregation kinetics of nanoplastics in aquatic systems. Water Res. 186, 116316.
Luo, L., Chen, Z., Lv, J., Cheng, Y., Wu, T., Huang, R., 2019. Molecular understanding of dissolved black carbon sorption in soil-water environment. Water Res. 154, 210–216.
Mao, Y., Ai, H., Chen, Y., Zhang, Z., Zeng, P., Kang, L., Li, W., Gu, W., He, Q., Li, H., 2018. Phytoplankton response to polystyrene microplastics: perspective from an entire growth period. Chemosphere 208, 59–68.
Mao, Y., Li, H., Gu, W., Yang, G., Liu, Y., He, Q., 2020a. Distribution and characteristics of microplastics in the Yulin River, China: role of environmental and spatial factors. Environ. Pollut. 265 (Pt A), 115033.
Mao, Y., Li, H., Huangfu, X., Liu, Y., He, Q., 2020b. Nanoplastics display strong stability in aqueous environments: insights from aggregation behaviour and theoretical calculations. Environ. Pollut. 258, 113760.
Mitrano, D.M., Wick, P., Nowack, B., 2021. Placing nanoplastics in the context of global plastic pollution. Nat. Nanotechnol. 16 (5), 491–500.
Ou, Q., Xu, Y., He, Q., Wu, Z., Ma, J., Huangfu, X., 2021. Deposition behavior of dissolved black carbon on representative surfaces: role of molecular conformation. J. Environ. Chem. Eng. 9 (5).
Phong, D.D., Hur, J., 2018. Using Two-dimensional correlation size exclusion chromatography (2D-CoSEC) and EEM-PARAFAC to explore the heterogeneous adsorption behavior of humic substances on nanoparticles with respect to molecular sizes. Environ. Sci. Technol. 52 (2), 427–435.
Porter, A., Lyons, B.P., Galloway, T.S., Lewis, C., 2018. Role of marine snows in microplastic fate and bioavailability. Environ. Sci. Technol. 52 (12), 7111–7119.
Qu, i., Hwang, Y.S., Alvarez, P.J.J., Bouchar, D., Li, Q., 2010a. UV Irradiation and humic acid mediate aggregation of aqueous fullerene (nC(60)) nanoparticles. Environ. Sci. Technol. 44 (20), 7821–7826.
Qu, X., Fu, H., Mao, J., Ran, Y., Zhang, D., Zhu, D, 2016. Chemical and structural properties of dissolved black carbon released from biochars. Carbon N Y 96, 759–767.
Qu, X., Hwang, Y.S., Alvarez, P.J.J., Bouchard, D., Li, Q., 2010b. UV Irradiation and humic acid mediate aggregation of aqueous fullerene (nC(60)) nanoparticles. Environ. Sci. Technol. 44 (20), 7821–7826.
Quigg, A., Santschi, P.H., Burd, A., Chin, W.C., Kamalanathan, M., Xu, C., Ziervogel, K., 2021. From nano-gels to marine snow: a synthesis of gel formation processes and modeling efforts involved with particle flux in the ocean. Gels 7 (3).
Shams, M., Alam, I., Chowdhury, I., 2020. Aggregation and stability of nanoscale plastics in aquatic environment. Water Res. 171, 115401.
Sun, B., Zhang, Y., Li, R., Wang, K., Xiao, B., Yang, Y., Wang, J., Zhu, L., 2021a. New insights into the colloidal stability of graphene oxide in aquatic environment: interplays of photoaging and proteins. Water Res. 200, 117213.
Sun, L., Chin, W.-.C., Chiu, M.-.H., Xu, C., Lin, P., A.Schwehr, K., Quigg, A., H.Santschi, P, 2019. Sunlight induced aggregation of dissolved organic matter: role ofproteins in linking organic carbon and nitrogen cycling in seawater. Sci. Total Environ. 654, 872–877.
Sun, L., Xu, C., Lin, P., Quigg, A., Chin, W.-.C., Santschi, P.H., 2021b. Photo-oxidation of proteins facilitates the preservation of high molecular weight dissolved organic nitrogen in the ocean. Mar. Chem. 229.
Sun, L., Xu, C., Zhang, S., Lin, P., Schwehr, K.A., Quigg, A., Chiu, M.H., Chin, W.C., Santschi, P.H., 2017. Light-induced aggregation of microbial exopolymeric substances. Chemosphere 181, 675–681.
Ter Halle, A., Jeanneau, L., Martignac, M., Jarde, E., Pedrono, B., Brach, L., Gigault, J., 2017. Nanoplastic in the North Atlantic subtropical gyre. Environ. Sci. Technol. 51 (23), 13689–13697.
Wang, J., Zhao, X., Wu, A., Tang, Z., Niu, L., Wu, F., Wang, F., Zhao, T., Fu, Z., 2021. Aggregation and stability of sulfate-modified polystyrene nanoplastics in synthetic and natural waters. Environ. Pollut. 268 (Pt A), 114240.
Wang, Y., Zhang, W., Shang, J., Shen, C., Joseph, S.D., 2019. Chemical aging changed aggregation kinetics and transport of biochar colloids. Environ. Sci. Technol. 53 (14), 8136–8146.
Wheeler, K.E., Chetwynd, A.J., Fahy, K.M., Hong, B.S., Tochihuitl, J.A., Foster, L.A., Lynch, I., 2021. Environmental dimensions of the protein corona. Nat. Nanotechnol. 16, 617–629.
Wu, H., Xu, X., Shi, L., Yin, Y., Zhang, L.C., Wu, Z., Duan, X., Wang, S., Sun, H., 2019a. Manganese oxide integrated catalytic ceramic membrane for degradation of organic pollutants using sulfate radicals. Water Res. 167, 115110.
Wu, J., Jiang, R., Lin, W., Ouyang, G., 2019b. Effect of salinity and humic acid on the aggregation and toxicity of polystyrene nanoplastics with different functional groups and charges. Environ. Pollut. 245, 836–843.
Wu, X., Liu, P., Gong, Z., Wang, H., Huang, H., Shi, Y., Zhao, X., Gao, S., 2021. Humic acid and fulvic acid hinder long-term weathering of microplastics in lake water. Environ. Sci. Technol.
Xu, H., Cooper, W.J., Jung, J., Song, W., 2011. Photosensitized degradation of amoxicillin in natural organic matter isolate solutions. Water Res. 45 (2), 632–638.
Xu, Y., Ou, Q., He, Q., Wu, Z., Ma, J., Huangfu, X., 2021. Influence of dissolved black carbon on the aggregation and deposition of polystyrene nanoplastics: comparison with dissolved humic acid. Water Res. 196, 117054.
Xu, Y., Ou, Q., Jiao, M., Liu, G., van der Hoek, J.P., 2022. Identification and quantification of nanoplastics in surface water and groundwater by pyrolysis gas chromatography-Mass Spectrometry. Environ. Sci. Technol. 56 (8), 4988–4997.
Xu, Y., Ou, Q., Liu, C., Zhou, X., He, Q., Wu, Z., Huang, R., Ma, J., Lu, D., Huangfu, X., 2020. Aggregation and deposition behaviors of dissolved black carbon with coexisting heavy metals in aquatic solution. Environmental Science: Nano.
Yu, S., Shen, M., Li, S., Fu, Y., Zhang, D., Liu, H., Liu, J., 2019. Aggregation kinetics of different surface-modified polystyrene nanoparticles in monovalent and divalent electrolytes. Environ. Pollut. 255 (Pt 2), 113302.
Zhang, Y.N., Cheng, F., Zhang, T., Li, C., Qu, J., Chen, J., Peijnenburg, W., 2022. Dissolved organic matter enhanced the aggregation and oxidation of nanoplastics under simulated sunlight irradiation in water. Environ. Sci. Technol. 56 (5), 3085–3095.
Zhang, Y.N., Wang, J., Chen, J., Zhou, C., Xie, Q., 2018. Phototransformation of 2,3-Dibromopropyl-2,4,6-tribromophenyl ether (DPTE) in natural waters: important roles of dissolved organic matter and chloride ion. Environ. Sci. Technol. 52 (18), 10490–10499.
Zhou, H., Lian, L., Yan, S., Song, W., 2017. Insights into the photo-induced formation of reactive intermediates from effluent organic matter: the role of chemical constituents. Water Res. 112, 120–128.